Computational Materials Science 128 (2017) 198–206

Contents lists available at ScienceDirect

Computational Materials Science

journal homepage: www.elsevier.com/locate/commatsci

Atomic ordering in Cu-Al-Ni: Point approximation and Monte Carlo simulations

F. Lanzini

Instituto de Física de Materiales Tandil (IFIMAT), Universidad Nacional del Centro de la Provincia de Buenos Aires (UNCPBA), and Consejo Nacional de Investigaciones Científicas y Técnicas (CONICET), Pinto 399, 7000 Tandil, Argentina

ARTICLE INFO

Article history:
Received 9 June 2016
Received in revised form 19 October 2016
Accepted 19 November 2016

Keywords:
Cu-Al-Ni
Atomic ordering
Monte Carlo simulations

ABSTRACT

Long range ordering in the bcc phase of the Cu-Al-Ni alloy is modelled through the analytical Bragg-Williams approximation and by means of numerical Monte Carlo simulations. The interchange energies that govern the ordering reactions are determined by fits to experimental ordering temperatures. A satisfactory agreement with the experimental data is obtained within both models, using slightly different sets of interchange energies. It is found that ordering in first neighbours is driven by the Ni-Al interactions, whereas the ordering in next nearest neighbours occurs by a reordering of Cu-Al pairs. Monte Carlo simulations enable a reinterpretation of the experimentally observed ordering reactions. Further details of the ordering process, such as the existence of tricritical points as the Ni content is reduced, and the evolution of sublattice occupancies as the ordering proceeds are also discussed: the site occupation probabilities at low temperatures agree with the experimental values.

1. Introduction

Cu-Al-Ni, as other Cu-Al based alloys, has shape memory properties associated with a martensitic transformation. This transformation takes place from a high temperature β phase, with bcc structure, to a low temperature martensitic phase. At temperatures above the martensitic transformation, the β phase can be in different states of long range order (*lro*). For instance, in the range of experimentally investigated compositions, the Cu-Al-Ni alloy undergoes a two stages ordering process: first from a disordered (or short range ordered) bcc structure, called *A*2, to a *B*2 structure ordered in first neighbours, and then to a $L2_1$ phase with order in first and second neighbours [1,2]. The type and degree of order in the β phase modifies the properties associated with the martensitic transformation [3]; thus, the understanding of the ordering processes is of interest from both basic and applied points of view.

The description of the different superstructures can be made with the help of Fig. 1, which shows the general bcc lattice and the four interpenetrating fcc sublattices (I to IV) in which it is subdivided. In the *A*2 structure all the sites have the same probability of being occupied by any of the atomic species, $p_A^I = p_A^{II} = p_A^{III} = p_A^{IV}$ (*A* = Cu, Al, Ni). In the *B*2 structure (ClCs type), the occupation of the center of the cubes differs from that of the corners, $p_A^I = p_A^{II} \neq p_A^{III} = p_A^{IV}$. In the $L2_1$ configuration (Heusler type structure), there is an additional ordering in second neighbours, $p_A^I = p_A^{II} \neq p_A^{III} \neq p_A^{IV} \neq p_A^I$.

The most comprehensive experimental assessment of critical order-disorder temperatures in Cu-Al-Ni is the work by Recarte et al. [4]. These authors measured critical order-disorder temperatures along three lines of compositions with fixed 13.2 wt% Al, 13.7 wt% Al, and 4 wt% Ni, respectively. For all the investigated samples, two ordering reactions were observed, that the authors identified with A2 → B2 and B2 → $L2_1$ ordering processes.

From the theoretical side, there have been three previous attempts to model the temperatures of atomic long range ordering in Cu-Al-Ni [4–6]. These studies were based on mean field approximations. In Ref. [4], expressions derived from the point (Bragg-Williams, BW) approximation [7] were used. It was assumed that the chemical interactions between *AB* pairs were determined by constant (composition and temperature independent) pair interchange energies in first and second neighbours, $W_{AB}^{(k)}$ (*AB* = CuAl, CuNi or AlNi, *k* = 1, 2 for first and second neighbours, respectively). The values for $W_{\mathrm{CuAl}}^{(1,2)}$ were taken from [8], $W_{\mathrm{AlNi}}^{(1,2)}$ from [9], and it was assumed that $W_{\mathrm{CuNi}}^{(1,2)} = 0$. In Ref. [5], the BW model, as modified by Inden [7] was used to model the *A*2 + *B*2 and *B*2 + *B*2 coexistence regions observed experimentally at low temperatures. The interchange energies in first and second neighbours for Cu-Al and Ni-Al were obtained from the (extrapolated) order-disorder temperatures in the corresponding binary alloys, whereas for Cu-Ni pairs they were assumed to be zero. More recently, a model based

E-mail address: flanzini@exa.unicen.edu.ar

http://dx.doi.org/10.1016/j.commatsci.2016.11.029
0927-0256/

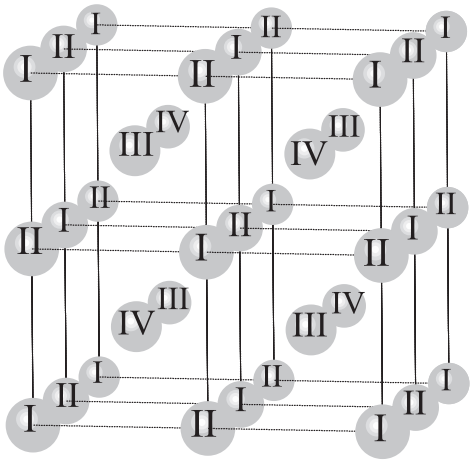

Fig. 1. The bcc lattice and the four interpenetrating sublattices in which it is subdivided.

in the irregular tetrahedron approximation of the cluster variation method (IT-CVM) [10] was employed by Pelegrina [6] to determine a new set of interchange energies from a fit to the experimental critical temperatures.

Despite these previous theoretical efforts, there are some issues that still remain unclear. One of them is the fact that, in all the range of compositions experimentally studied, Cu-Al-Ni displays a two-steps ordering process even for very low Ni contents (2.73 at.%, [4]). This contrasts with the behaviour of other Cu-Al-X ternary alloys (X = Zn, Be, Mn), which, for low contents of the third element X (below ≈8 at.%), display a single $A2 \leftrightarrow L2_1$ transition [27–31], consistently with the fact that Cu-Al with compositions close to Cu_3Al has also a single ordering transition [23]. The different behaviour of Cu-Al-Ni could be attributed, in principle, to a high binding energy for Ni-Al pairs. One of the objectives of the present work is the construction of realistic model which can clarify this and other points.

The BW model has the advantage of its relatively easy application to the problem of atomic ordering, and, in particular, provides analytical expressions for the determination of interchange energies by fitting to experimental order-disorder temperatures. However, since this model neglects short range order correlations, the thermodynamical quantities obtained within this approach considerably differs from the results obtained with more realistic methods [11]; this has been shown to occur, for instance, in the related ternary Cu-Al-Zn system [12]. A more sophisticated approach is the Monte Carlo (MC) method, which allows obtaining quasi-exact results from calculations made on finite systems [13]. However, due to the numerical character of this technique, it may become difficult determining the interaction parameters from a fit to experimental data, such as order-disorder transition temperatures. A plausible solution, which will be employed in the present work, is to use the interchange energies obtained within the BW model as initial guesses for the MC simulations [11]. This initial values should be optimized in order to obtain an adequate description of the experimental order-disorder temperatures.

The purpose of the present work is the construction of a model for the description of ordering phenomena in Cu-Al-Ni. The interchange energies are determined by fitting to the experimental order-disorder temperatures from Ref. [4]. The BW formalism, as described in Section 2.1, is used as first approximation, and the values are further optimized for their use in MC simulations (described in Section 2.2). Two types of MC simulations are performed: first, canonical ensemble simulations with direct atomic interchanges are used to optimize the energetic parameters and to analyze the predicted atomic distributions. Then, the phase equilibrium around the compositions of interest is studied by means of simulations in the grand-canonical ensemble. The rest of this paper is organized as follows: in Sections 3.1 and 3.2 we present and discuss the results obtained with BW and MC, respectively; the validity of the MC model is analyzed by comparing with other experimental information not included in the fitting. The main conclusions are drawn in Section 4.

2. Theory

2.1. Bragg-Williams model

The Bragg-Williams (BW) [7] model is the lowest step in a hierarchy of successive approximations to the free energy of an alloy known as the Cluster Variation Method (CVM) [10]: In this approximation, the configurational free energy is written in terms of the probabilities p_i^α for a site in sublattice α ($\alpha = I - IV$) to be occupied by an atom of specie i. Since probabilities of larger clusters (for instance, pair probabilities) are given just in terms of the p_i^α's, this is also known as the *point* approximation of the CVM [11,14]. For a bcc ternary alloy A-B-C with atomic fractions c_A, c_B and c_C, and considering constant pair interactions extended to first and second neighbours, the configurational free energy per atom, F/N, takes the form [15]:

$$\frac{F}{N} = \frac{U - TS}{N} = \sum_{ij}\left[4x_i x_j W_{ij}^{(1)} - 3\left(x_i x_j - \frac{1}{2}(y_i y_j + z_i z_j)\right)W_{ij}^{(2)}\right] + \sum_{ij} c_i c_j\left(-4W_{ij}^{(1)} - 3W_{ij}^{(2)}\right) + \sum_i c_i\left(4V_{ii}^{(1)} + 3V_{ii}^{(2)}\right) + \frac{k_B T}{4}\sum_{\alpha=I}^{IV} p_i^\alpha \cdot \ln\left(p_i^\alpha\right) \quad (1)$$

In the above expression, U is the internal energy, T is the absolute temperature and S the entropy; $V_{ii}^{(k)}$ is the interaction between a pair of $i - i$ atoms placed as first ($k = 1$) or second ($k = 2$) neighbours; $W_{ij}^{(k)} = -2V_{ij}^{(k)} + V_{ii}^{(k)} + V_{jj}^{(k)}$ are the so-called *interchange energies*, which determine the tendency to ordering or segregation between the components i and j. The parameters x_i are linear combinations of probabilities and quantify the degree of order in first neighbours

$$x_i = \frac{p_i^I + p_i^{II} - p_i^{III} - p_i^{IV}}{4} \quad (2\text{-a})$$

whereas y_i and z_i are linear combinations that describe the ordering between second neighbours,

$$y_i = \frac{p_i^I - p_i^{II}}{2} \quad (2\text{ - b})$$

$$z_i = \frac{p_i^{III} - p_i^{IV}}{2} \quad (2\text{-c})$$

Due to the conditions $\sum_i p_i^\alpha = 1$, and $\sum_\alpha p_i^\alpha = 4c_i$, only six among the twelve occupation probabilities are independent; the description of the type and degree of *lro* is then more conveniently performed through the six independent parameters x_i, y_i and z_i ($i = A$, B; $x_C = -x_A - x_B$, $y_C = -y_A - y_B$, $z_C = -z_A - z_B$). Thus, in absence of *lro* (structure $A2$), is $x_i = y_i = z_i = 0$; in a $B2$ configuration, ordered in first neighbours, is $x_i \neq 0$, $y_i = z_i = 0$; and for an $L2_1$ structure is $x_i \neq 0$, $z_i \neq 0$, and $y_i = 0$.

In Eq. (1), the first term accounts for the energy due to ordering, the second one is the energy due to mixing, the third one is the internal energy of the pure components, and the last one is the configurational entropy (k_B being the Boltzmann's constant). The summations run over $i = A$, B, and C, or over $ij = AB$, AC, BC.

Since in equilibrium the free energy is a minimum, its derivative with respect to the order parameters is zero. Particularly, in the temperature region between $T_{A2\leftrightarrow B2}$ and $T_{B2\leftrightarrow L2_1}$, where some degree of order in first (but not in second) neighbours exists, the equilibrium conditions

$$\frac{\partial F}{\partial x_A} = N\left\{-\Xi_{AC}x_A + \frac{1}{2}(\Xi_{AB}-\Xi_{AC}-\Xi_{BC})x_B + \frac{1}{2}k_BT\cdot\ln\left[\frac{(c_A+x_A)(c_C+x_A+x_B)}{(c_A-x_A)(c_C-x_A-x_B)}\right]\right\} = 0 \quad (3\text{ - a})$$

$$\frac{\partial F}{\partial x_B} = N\left\{-\Xi_{BC}x_B + \frac{1}{2}(\Xi_{AB}-\Xi_{AC}-\Xi_{BC})x_A + \frac{1}{2}k_BT\cdot\ln\left[\frac{(c_B+x_B)(c_C+x_A+x_B)}{(c_B-x_B)(c_C-x_A-x_B)}\right]\right\} = 0 \quad (3\text{-b})$$

admit other solutions beside the trivial $x_A = x_B = 0$. In the preceding expressions,

$$\Xi_{ij} = \left(8W_{ij}^{(1)} - 6W_{ij}^{(2)}\right)_{BW}. \quad (4)$$

The critical temperature for ordering in first neighbours is given by the condition [7,15,16]

$$\left[\frac{\partial^2 F}{\partial x_A^2}\frac{\partial^2 F}{\partial x_B^2} - \left(\frac{\partial^2 F}{\partial x_A \partial x_B}\right)^2\right]_{x_A=x_B=y_A=y_B=z_A=z_B=0} = 0$$

leading to

$$k_BT_{A2\leftrightarrow B2}^{BW} = 0.5\cdot\left\{\sum_{ij}c_ic_j\Xi_{ij} + \sqrt{\left(\sum_{ij}c_ic_j\Xi_{ij}\right)^2 - 4c_Ac_Bc_C\left(\Xi_{AC}\Xi_{BC} - \frac{1}{4}[\Xi_{AC}+\Xi_{BC}-\Xi_{AB}]^2\right)}\right\} \quad (5)$$

Analogously, the critical temperature for the $B2\leftrightarrow L2_1$ transition is given by the condition

$$\left[\frac{\partial^2 F}{\partial z_A^2}\frac{\partial^2 F}{\partial z_B^2} - \left(\frac{\partial^2 F}{\partial z_A \partial z_B}\right)^2\right]_{y_A=y_B=z_A=z_B=0} = 0$$

which gives

$$k_BT_{B2\leftrightarrow L2_1}^{BW} = 3\left\{\Omega + \sqrt{\Omega^2 - \left(4W_{AC}^{(2)}W_{BC}^{(2)} - \left[W_{AC}^{(2)}+W_{BC}^{(2)}-W_{AB}^{(2)}\right]^2\right)_{BW}\cdot\sum_i(c_i-x_i)}\right\} \quad (6)$$

where

$$\Omega = \left(W_{AC}^{(2)}\right)_{BW}(c_B+c_C+x_A)(c_A-x_A) + \left(W_{BC}^{(2)}\right)_{BW}(c_A+c_C+x_B)(c_B-x_B) - \left(W_{AC}^{(2)}+W_{BC}^{(2)}-W_{AB}^{(2)}\right)_{BW}(c_B-x_B)(c_A-x_A) \quad (7)$$

In this work, the calculation of the interchange energies using the BW formalism was performed in three steps: (a) fit to the experimental $T_{A2\leftrightarrow B2}$'s with expression (5) thus determining the Ξ_{ij}'s; (b) for each composition, numerical calculation of the first neighbours order parameters x_{Cu} and x_{Ni} at the experimental $T_{B2\leftrightarrow L2_1}$ ($x_{Al} = -x_{Cu} - x_{Ni}$), using Eqs. (3); (c) using these values of the x_i's, determination of the $\left(W_{ij}^{(2)}\right)_{BW}$ by fitting to the experimental $T_{B2\leftrightarrow L2_1}$ using Eqs. (6) and (7).

2.1.1. Short-range order corrections

Since the BW model disregard any kind of short range order correlation [17], fitting to experimental results with expressions obtained within this model leads to the prediction of interchange energies that are lower than the values obtained by more realistic methods (MC simulations or IT-CVM, for instance). Conversely, for given values of the interchange energies, replacement in the BW expressions (1)–(7) results in the prediction of critical temperatures that are higher than those obtained by other methods. In order to solve this drawback, Inden [7,17] proposed an *a posteriori* correction of the pair interchange energies by a constant factor χ_{ij}:

$$W_{ij}^{(k)} = \frac{\left(W_{ij}^{(k)}\right)_{BW}}{\chi_{ij}} \quad (8)$$

Here, $\left(W_{ij}^{(k)}\right)_{BW}$ are the energies obtained within the BW formalism, and the $W_{ij}^{(k)}$ are the corrected values. The factors χ_{ij} are different for different binary subsystems, and depend on the ratio $W_{ij}^{(2)}/W_{ij}^{(1)} = \left(W_{ij}^{(2)}\right)_{BW}/\left(W_{ij}^{(1)}\right)_{BW}$ [7,9].

2.2. Monte Carlo method

The Monte Carlo method applied to the problem of ordering or segregation in alloys is based on the computational simulation of a crystal lattice [18,19] Each site i of the virtual crystal is associated with a variable σ_i representing the atomic species. For our ternary alloy, we used $\sigma_i = +1$, 0, or -1 to represent Cu, Ni or Al atoms, respectively. The configurational energy of the alloy is given by the Ising-like Hamiltonian [20]

$$\mathcal{H} = \sum_{ij}^{n.n.}\left\{J_1\sigma_i\sigma_j + K_1\sigma_i^2\sigma_j^2 + L_1\left(\sigma_i^2\sigma_j + \sigma_i\sigma_j^2\right)\right\} + \sum_{ij}^{n.n.n.}\left\{J_2\sigma_i\sigma_j + K_2\sigma_i^2\sigma_j^2 + L_2\left(\sigma_i^2\sigma_j + \sigma_i\sigma_j^2\right)\right\} \quad (9)$$

The first summation extends to ij pairs placed as nearest neighbours and the second to next-nearest neighbours. The constants J_i, K_i and L_i are related to the interchange energies:

$$J_i = \frac{1}{4}W_{AB}^{(i)}, \quad K_i = \frac{1}{4}\left(2W_{AC}^{(i)} + 2W_{BC}^{(i)} - W_{AB}^{(i)}\right), \quad L_i = \frac{1}{4}\left(W_{AC}^{(i)} - W_{BC}^{(i)}\right) \quad (10)$$

Simulations in both the canonical and semi-grand canonical ensembles were performed. In all the calculations, lattices comprising 2×32^3 atomic sites (for which finite size effects are negligible) were used. A few tests using lattices with 2×64^3 yielded almost identical results.

2.2.1. Canonical ensemble simulations

The simulation of the ordering process was performed as follows: from a given site i, one of his eight nearest neighbours, j, was selected at random. The probability p of a direct atomic interchange, $\sigma_i' = \sigma_j$, $\sigma_j' = \sigma_i$, (where the primes are the values of the occupation variables after the interchange) was evaluated through the standard Metropolis algorithm [21]:

$$p = \max\left\{1, \exp\left(-\frac{\Delta E}{k_BT}\right)\right\} \quad (11)$$

i.e., the interchange was accepted if the new configuration has lower energy than the initial ($\Delta E = E' - E \leqslant 0$) and was accepted with a probability $\exp\left(-\frac{\Delta E}{k_BT}\right)$ if $\Delta E > 0$. Here, k_B is the Boltzmann constant, T is the absolute temperature, and the energies are evaluated by means of Eqs. (9) and (10). A number of $2\times L^3$

attempts of interchange was defined as a Monte Carlo step (MCs) (L = 32 or 64 is the side of the virtual box).

In order to test whether the use of this direct atomic interchange mechanism could influence the calculated equilibrium properties, a vacancy-mediated mechanism was implemented. In this case, a vacancy was introduced at random in the crystal, and only vacancy-atom interchanges were allowed. The computation of the energy for the 'ternary alloy plus vacancy' system was done as for a four component alloy in which the interaction energy of the vacancy with any of the atomic species was assumed to be zero.

2.2.2. Semi-grand canonical ensemble simulations

In semi-grand canonical (SGC) simulations the chemical composition of the lattice do not remain constant; instead, it is modified according to the chemical potential μ of the atomic species. For fixed values of the temperature and chemical potentials, the simulation proceeds as follows: given an atomic site i, the probability of replacing the atom σ_i by a new species σ_i' is calculated by means of the modified Metropolis algorithm:

$$p = \max\left\{1, \exp\left(-\frac{\Delta E - \sum_A \mu_A \Delta N_A}{k_B T}\right)\right\} \quad (12)$$

where the subscript A refers to the different atomic species (A = Cu, Ni, Al), N_A is the number of atoms of each species, and μ_A is the corresponding chemical potential. Note that since the total number of atoms remains constant, the summation can be reduced to a two-term summation with a straightforward redefinition of the chemical potentials. In the SGC simulations, a MC step was defined as a set of $2 \times L^3$ replacement attempts.

2.2.3. Calculation of observables

Several observables of the system, such as long and short range order parameters, energy, or entropy [12] can be extracted from the simulations. In the canonical ensemble, for a fixed value of the temperature T, the evolution of the system was monitored by evaluating the *lro* parameters defined in Eqs. 2(a–c) and also the accumulated variation of energy. For a given T, it requires a certain number of MC steps to reach the equilibrium configuration, i.e., the situation in which no further evolution of the parameters of interest is observed. After the equilibrium is attained, the simulation continues in order to obtain statistical averages of the quantities of interest. For canonical simulations with direct atomic interchange mechanism, the number of MCs necessary to guarantee the equilibration was of the order of 5×10^4 MCs at each temperature. Due to critical slowing down, this number was sometimes increased in the vicinity of the critical temperatures. For the vacancy-mediated mechanism, the number of MCs necessary to reach equilibrium increases significantly. In semi-grand canonical simulations, besides the *lro* parameters, also the atomic content c_i of each species is a by-product of the simulation.

It should be noted that, when the alloy under study is an inhomogeneous state (for instance, coexistence of different phases or different variants of the same phase), the procedure of averaging over the entire lattice in the canonical ensemble can lead to misleading results. A way to circumvent this drawback is to subdivide the lattice in smaller cubes, and to calculate the value of the order parameters for each of this cubes [22].

3. Results and discussion

3.1. Bragg-Williams model

The fit to the experimental order-disorder temperatures with the BW expressions was done in the way detailed in Section 2.1. In order to reduce the number of adjustable parameters, we assumed $W^{(1)}_{CuNi} = W^{(2)}_{CuNi} = 0$. Although it has been reported that the interchange energies for Cu-Ni pairs are not exactly zero but slightly positive [24], this is a reasonable guess taking into consideration the absence of long range order in the binary Cu-Ni phase diagram. It should be noted, also, that in the only previous attempt

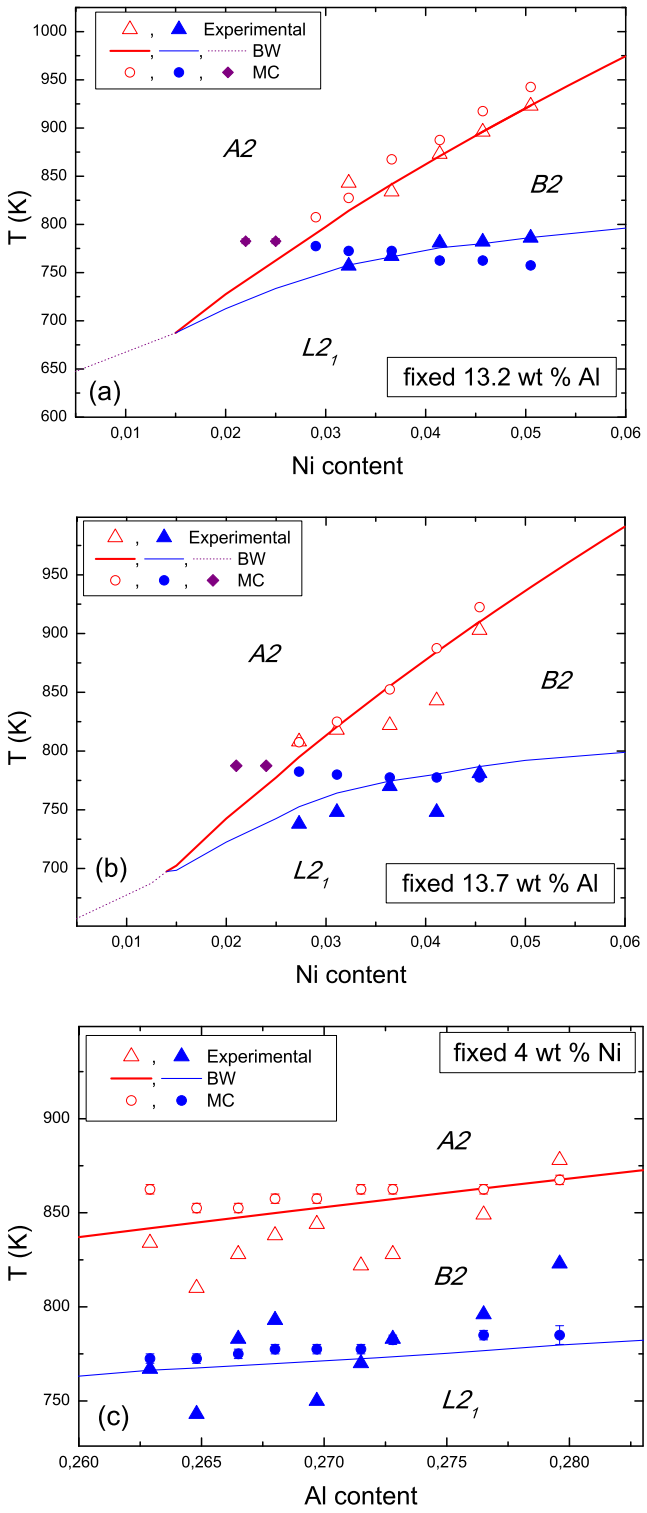

Fig. 2. Experimental order-disorder temperatures (from Ref. [4]), fits within the BW model, and MC calculations. The empty symbols correspond to the $A2 \leftrightarrow B2$ transition, and the solid ones to $B2 \leftrightarrow L2_1$. The diamonds and the dotted lines represent calculated $A2 \leftrightarrow L2_1$ transitions.

to determine these interchange energies [6], the values obtained were close to zero. Contrary to what was asserted by Pelegrina [6], we did not found here that improper atom configurations were stabilized under this restriction, since our calculations predict the correct ordering sequence in the range of compositions experimentally studied. Besides, due to the scattering in the experimental data, we included only the experimental order-disorder temperatures corresponding to compositions with fixed 13.2 wt.% Al. The inclusion of the remaining data leads to unphysical results (such as interchange energies diverging to very large negative or positive values). Despite this simplification, the agreement of our final results with the experimental data is satisfactory for the three lines of composition. The corresponding phase diagrams are displayed in Fig. 2a–c. In order to correct for short-range correlations, we applied the method detailed in Section 2.1.1. The ratio between the interchange energies for the binary subsystems were found to be $\frac{\left(W^{(2)}_{\mathrm{CuAl}}\right)^{BW}}{\left(W^{(1)}_{\mathrm{CuAl}}\right)^{BW}} = 0.69$, and $\frac{\left(W^{(2)}_{\mathrm{AlNi}}\right)^{BW}}{\left(W^{(1)}_{\mathrm{AlNi}}\right)^{BW}} = 0.54$. The corresponding corrective factors are, according to [7], $\chi_{\mathrm{CuAl}} \approx 0.59$ and $\chi_{\mathrm{AlNi}} \approx 0.68$. After correcting with Eq. (8), we obtained the values:

$$W^{(1)}_{\mathrm{CuAl}} = 1247k_B;\quad W^{(2)}_{\mathrm{CuAl}} = 864k_B;\quad W^{(1)}_{\mathrm{NiAl}} = 3929k_B;\quad W^{(2)}_{\mathrm{NiAl}} = 2110k_B. \tag{13}$$

The interchange energies obtained for the Cu-Al binary subsystem are in reasonable agreement with those obtained by other authors within the framework of the BW model [8]. For Ni-Al, the interchange energies obtained here are higher than previous estimations [4–6].

A remarkable feature in Fig. 2a and b is that, as the Ni content is reduced, the lines corresponding to $T_{A2\leftrightarrow B2}$ and $T_{B2\leftrightarrow L2_1}$ coalesce into a single $A2 \leftrightarrow L2_1$ transition (dotted lines). The $T_{A2\leftrightarrow L2_1}$ transition lines have been calculated by numerical minimization of the free energy, Eq. (1). The existence of a single transition for low Ni contents is consistent with experimental and theoretical results

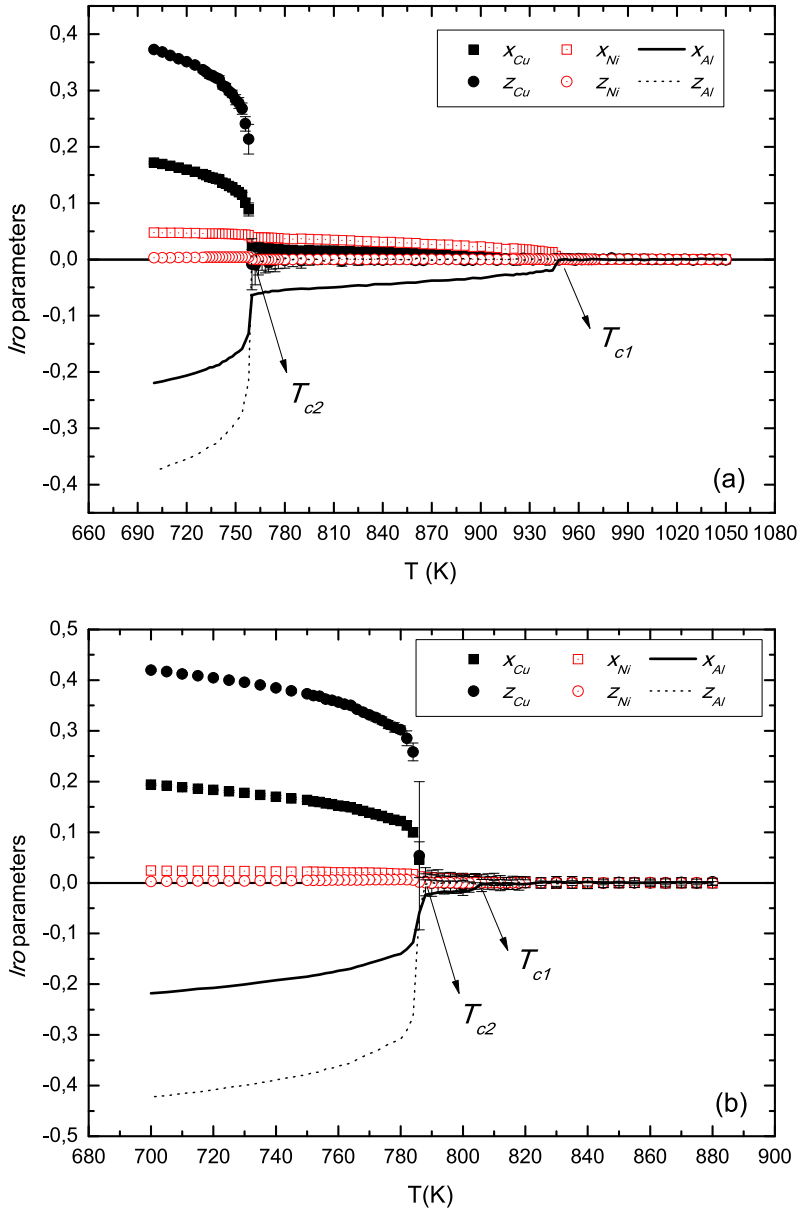

Fig. 3. Thermal evolution of the *lro* parameters (Eqs. (2a-c)) for (a) Cu – 26.26 at.% Al – 5.05 at.% Ni, and (b) Cu – 27.16 at.% Al – 2.73 at.% Ni. The parameters y_i, Eq. (2-b), are not shown since they are zero in all the range of temperatures.

in the binary Cu-Al system [23–26] and also in ternary Cu-Al-X alloys with low content of the third element (X = Zn, Mn, Be) [27–31].

3.2. Monte Carlo simulations

3.2.1. Canonical ensemble

Direct use of the BW energies (13) in MC simulations leads to simulated critical temperatures that do not agree with the experimental values. However, these energies can be used as a starting point, and then optimized to achieve the best possible fit [11]. The optimization was done by varying the interchange energies in the following way: keeping the energies for Cu-Ni pairs equal to zero, the remaining four energies were varied by trial-and-error until a minimum in the summation of the squared difference between calculated and measured critical temperatures was reached. In order to reduce the computation time, only the two extreme compositions for each of the three lines shown in Fig. 2 were used in the optimization. Following this procedure, we have found that the best fit to the experimental critical temperatures is obtained using the energies:

$$W^{(1)}_{\mathrm{CuAl}} = 1350k_B;\ W^{(2)}_{\mathrm{CuAl}} = 1000k_B;\ W^{(1)}_{\mathrm{NiAl}} = 3650k_B;\ W^{(2)}_{\mathrm{NiAl}} = 2100k_B. \tag{14}$$

The critical order-disorder temperatures obtained from the MC simulations are represented in Fig. 2. The simulations also show that the double ordering process join into a single reaction at low Ni contents (≈ 2.5 at.%). This single transition is represented by diamonds in Fig. 2a and b. Although the agreement between calculated and experimental critical temperatures is far from perfect, the general trend is well reproduced. It should be noted, besides, the considerable scatter in the experimental data.

In Fig. 3a and b we show the thermal evolution of the *lro* parameters defined in Eqs. (2) for alloys with compositions Cu – 26.26 at.% Al – 5.05 at.% Ni and Cu – 27.16 at.% Al – 2.73 at.% Ni. These compositions have been chosen since they are the ones with higher and lower Ni content among the alloys studied in [4]. The parameters y_i, Eq. (2-b), are not represented in Fig. 3 because they are identically zero in all the range of temperatures. The $A2 \rightarrow B2$ transition is characterized by a re-arrangement of Ni atoms towards sublattices I and II ($x_{\mathrm{Ni}} > 0$, see Eq. (2-a)), and, simultaneously, the occupation of sublattices III and IV by Al atoms ($x_{\mathrm{Al}} < 0$). On the other hand, in the *B*2 structure the Cu atoms remain almost uniformly distributed among the four sublattices ($x_{\mathrm{Cu}} \approx 0$). Thus, we can see that in this system the atomic ordering in nearest neighbours is driven by the formation of Ni-Al pairs. This mechanism contrasts with the alloys Cu-Al-Zn and Cu-Al-Mn, in which the ordering to *B*2 is driven by a rearrangement of Cu and Al pairs as nearest neighbours [12,28,29]. This is due to a higher value of $W^{(1)}_{\mathrm{NiAl}}$ with respect to $W^{(1)}_{\mathrm{CuAl}}$. Finally, during the second ordering reaction, a redistribution of Cu and Al pairs in sublattices III and IV occurs. These calculated ordering mechanisms agree with the mechanisms proposed by Nakata et al. [1].

It should be noted, however, that according to our simulations the passage from the disordered *A*2 configuration to the *B*2 structure occurs by a nucleation mechanism: a *B*2 region, with composition close to NiAl, forms in a disordered matrix. The matrix results impoverished in Ni and Al. At a lower temperature, this matrix further reorders in next-nearest neighbours. The process is represented in Fig. 4a–c, where snapshots of the equilibrium configuration of the alloy Cu – 26.26 at.% Al – 5.05 at.% Ni at three temperatures are shown. Fig. 4 represents two consecutive {1 0 0} planes of the bcc lattice. Fig. 4a shows the equilibrium configuration after 1×10^6 MC steps at T = 1000 K, i.e., above the uppermost

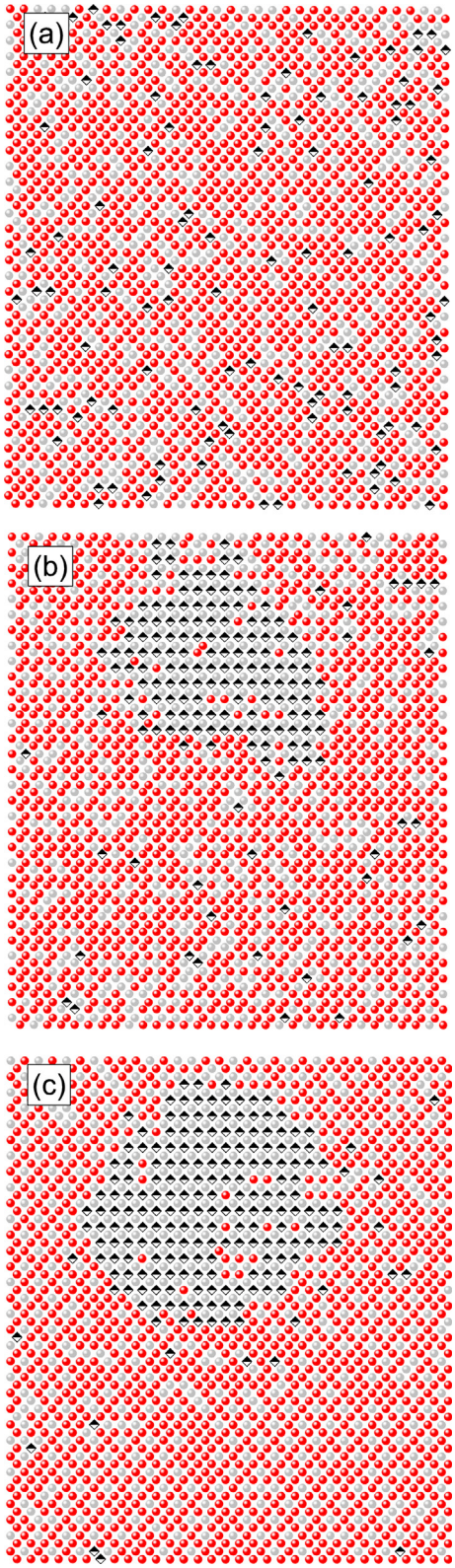

Fig. 4. Two consecutive {1 0 0} planes of the bcc lattice for an alloy Cu – 26.26 at.% Al – 5.05 at.% Ni at (a) T = 1000 K; (b) T = 850 K; (c) T = 700 K. Red spheres represent Cu atoms, light gray spheres represent Al, and black diamonds represent Ni. (For interpretation of the references to colour in this figure legend, the reader is referred to the web version of this article.)

ordering reaction (see Fig. 3a); there is no long range ordered structure. After equilibration at T = 850 K (Fig. 4b), a region with composition close to NiAl and with *B*2 order was formed in a dis-

ordered matrix; this temperature corresponds to a point between the first and second ordering reactions in Fig. 3a. Finally, at T = 700 K, also the matrix partially orders; this is appreciable in the lower part of Fig. 4c. The structure of the matrix is ordered in first and second neighbours, and with composition close to Cu_3Al.

According to the analysis of Fig. 4, as the temperature diminishes, the two consecutive ordering reactions predicted by the MC method should be regarded as the passage from a homogeneous *A*2 configuration to a *B*2 + *A*2 region, and then to a *B*2 + $L2_1$ two-phase field. This seems to be in contradiction with the analysis of Refs. [2,33], where a homogeneous distribution of the atomic species is found. On the other hand, it is worth to note that the existence of two phase fields has been reported both for the binary alloy with compositions around Cu_3Al [23,26], as well as for ternary Cu-Al-Ni with higher Ni contents (≈10–15 at.%) [5,32]. Additional calculations in the grand canonical ensemble are presented below.

Further verification of the validity of the present model can be obtained by comparing the predicted site occupation probabilities with experimental results. Pérez-Landazábal et al. [2] studied the atomic distribution at room temperature on a sample Cu – 27.4 at.% Al – 3.6 at.% Ni by means of neutron powder diffraction measurements. It was found that in the $L2_1$ structure the Al atoms tend to fulfill one of the sublattices (say sublattice IV in Fig. 1), with all the Ni atoms placed as first neighbours (sublattices I and II), and the Cu atoms occupying the remaining sites I, II and III. The excess Al tend to place in sublattice III. These authors obtained the site occupancies listed in Table 1, where they are compared with the average equilibrium values at T = 300 K obtained with the MC technique. The agreement between experimental and calculated results is satisfactory. In a recent paper [33], Nakata et al. determined, using powder X-ray analysis, the site occupation of an alloy Cu – 30.1 at.% Al – 3.6 at.% Ni at 473 K. Their results are compared with our MC results in Table 2. It should be noted, however, that the results of the MC simulations correspond to averaging over the matrix and the *B*2 precipitates (Fig. 4).

Another test of the validity of our model is obtained by comparing their predictions with experimental order-disorder temperatures not included in the fitting, i.e., with data from compositions outside the fitting composition range. In particular, Chen and Liu [34] studied by experimental methods an alloy Cu – 27.76 at.% Al

Table 1
Site occupation probabilities in Cu – 27.4 at.% Al – 3.6 at.% Ni at room temperature.

	Experimental [2]			MC, present work		
Sublattice	Cu	Al	Ni	Cu	Al	Ni
I, II	0.90(2)	0	0.10(2)	0.93	0	0.07
III	0.86(2)	0.14(2)	0	0.90	0.10	0
IV	0.04(2)	0.96(2)	0	0.01	0.99	0

Table 2
Site occupation probabilities in Cu – 30.1 at.% Al – 3.6 at.% Ni at 473 K.

	Experimental [33]			MC, present work		
Sublattice	Cu	Al	Ni	Cu	Al	Ni
I, II	0.853	0.075	0.072	0.886	0.042	0.072
III	0.895	0.105	0	0.874	0.126	0
IV	0.051	0.949	0	0.007	0.993	0

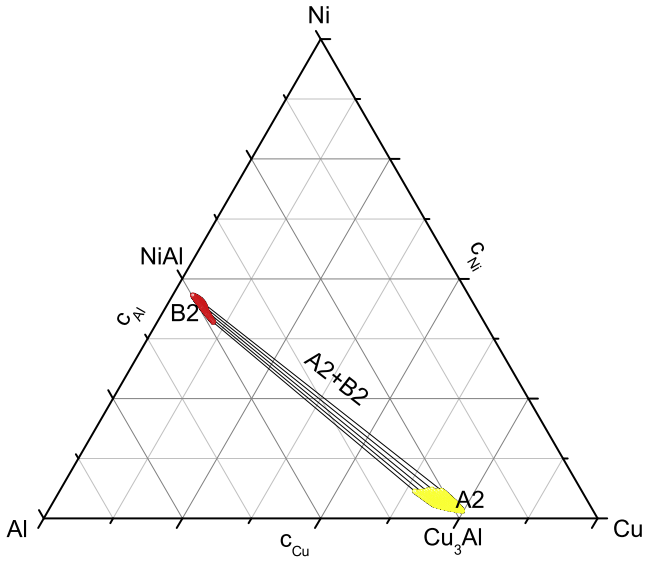

Fig. 5. Part of the isothermal section of the phase diagram at T = 1000 K.

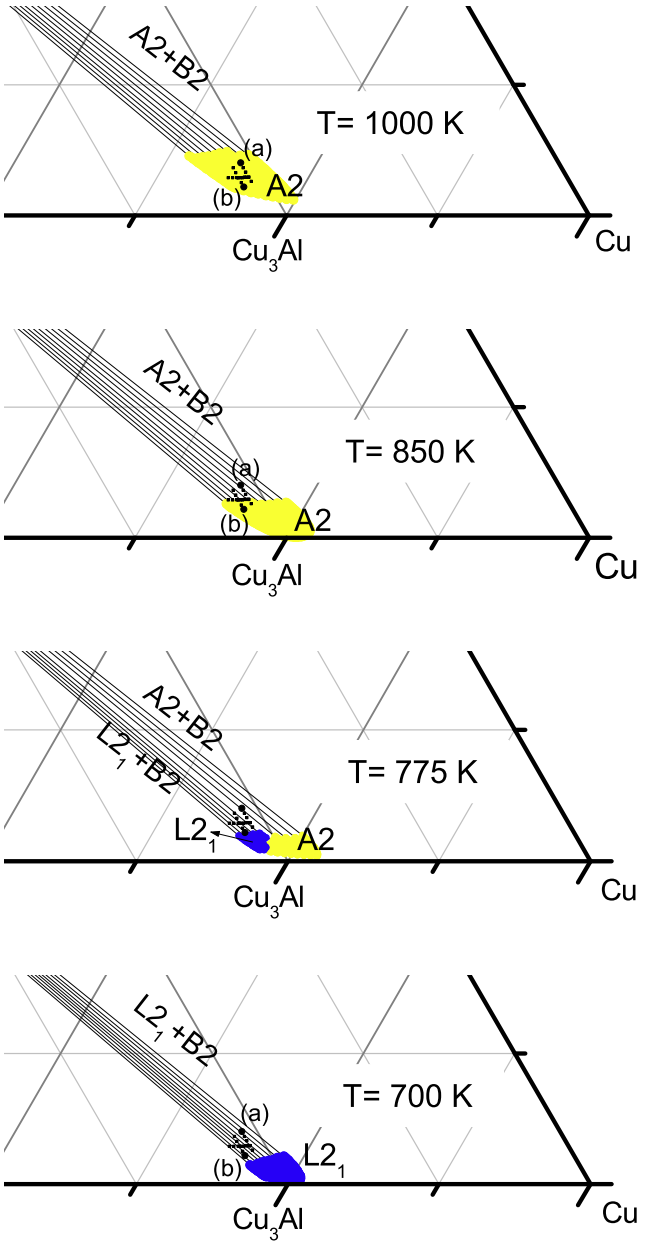

Fig. 6. Details of the isothermal sections of the phase diagram at T = 1000, 850, 775, and 700 K. The small black points represent the compositions of interest.

– 13.47 at.% Ni; they found that the critical $T_{A2\leftrightarrow B2}$ temperature is in the interval between 1248 and 1273 K. MC simulations using the energies (14) give $T_{A2\leftrightarrow B2} = 1222.5 \pm 2.5K$, in good agreement. It should be noted that this composition is far away from the compositions used in the fitting; this result further support the ability of the model presented here for extrapolation of critical temperatures.

All the previous results have been obtained using a direct atomic interchange mechanism. For comparison purposes, simulations with a vacancy-mediated mechanism were also implemented. Only the alloy with composition Cu – 26.26 at.% Al – 5.05 at.% Ni was studied by this method. Preliminary results indicate that the thermal evolution of the *lro* parameters is quite similar to that obtained with the direct interchange mechanism; also, snapshots of the atomic distribution at 1000, 850, and 700 K looks very similar to those shown in Fig. 4.

3.2.2. Semi-grand canonical ensemble

In order to obtain a more detailed picture of the ordering processes, simulations in the semi-grand canonical ensemble at several temperatures were performed. These calculations were restricted to the region of the phase diagram around the concentrations of interest. Fig. 5 shows a part of the ternary section at 1000 K.

The remarkable feature is the existence of a wide two-phase region. The coexisting phases have compositions close to stoichiometric NiAl and Cu_3Al. Whereas the compositions around NiAl have $B2$ ordering, those near Cu_3Al are disordered at 1000 K. In Fig. 6, details of the isothermal sections at T = 1000, 850, 775 and 700 K around the compositions of interest are presented. The compositions experimentally investigated in [2] are represented by small black dots. The dot labeled (a) corresponds to the same composition as in Figs. 3a and 4, and (b) corresponds to the composition of Fig. 3b. At T = 1000 K all the alloys of interest are in a homogeneous disordered A2 configuration. As the temperature decreases, the region of stability of this homogeneous phase decreases, and at T = 850 K, some of the alloys of interest enter in the $A2 + B2$ two-phase field. When the temperature is reduced further, the disordered matrix orders to a $L2_1$ configuration. Although not appreciable in the Figures, at T = 775 K a narrow coexistence gap separates de $A2$ and $L2_1$ stability regions. At T = 700 K, the alloys are in a $L2_1 + B2$ two-phase field. This picture is consistent with the calculations performed in the canonical ensemble, in particular with the results shown in Figs. 3 and 4.

4. Conclusions

In this work we presented two different theoretical methods for the study of order-disorder phenomena in Cu-Al-Ni. The first, simpler approach, is based in the analytical formulae obtained in the framework of the Bragg-Williams theory for ternary bcc alloys. By applying this method, a first approximation to the interchange energies in nearest and next-nearest neighbours was obtained (Eq. (13)). A second, more elaborated approach, consisted in the numerical simulation of the ordering processes by means of Monte Carlo simulations in the canonical and semi-grand canonical ensembles. The interchange energies used in this model were obtained by slight modification of the BW estimates (Eq. (14)). Within both methods, a satisfactory agreement with the experimental order-disorder temperatures was obtained.

It was found that the formation of a B2 structure is driven by the ordering of Ni-Al pairs, since their energetic interactions are stronger than those corresponding to Cu-Al or Cu-Ni pairs. This makes that the Cu-Al-Ni system behave differently to other Cu-Al-X bcc alloys previously studied, for which the interchange energies of Cu-Al pairs dominate. In particular, this explain why Cu-Al-Ni displays a double ordering process even for very low contents of Ni. Our calculations predict that the $A2 \leftrightarrow B2$ and $B2 \leftrightarrow L2_1$ transitions join into a single $A2 \leftrightarrow L2_1$ transition at Ni contents lower than those experimentally investigated.

The average site occupation probabilities obtained by means of MC simulations satisfactorily agree with the experimental values reported in Ref. [2] for a sample Cu – 27.4 at.% Al – 3.6 at.% Ni at room temperature, and with those from [33] for Cu – 30.1 at.% Al – 3.6 at.% Ni at 473 K.

From the calculations in the semi-grand canonical ensemble it is concluded that, according to the model, the first ordering reaction as the temperature decreases corresponds to the nucleation of $B2$ particles with composition close to NiAl in a disordered matrix; the second reaction originates from the ordering of the matrix to a $L2_1$ structure. The prediction of inhomogeneous $B2$ ordering seems to be in contradiction with experimental studies in this range of compositions [2,33], but is consistent with reports of an $A2 + B2$ two phase field at higher Ni contents [5,32].

Finally, it is worth to remark some of the limitations of the model developed here, and to comment on some possible improvements. First, the present model restrict the atomic interactions to only nearest and next-nearest neighbours pairwise energies: whereas it is known that these are the dominant contributions to the internal energy in bcc and fcc transition metal alloys (see Ref. [11], page 517), the model can be improved by including more distant pairs and multiplet (triplet, tetrahedra) interactions. Secondly, it has been assumed that the interchange energies are independents on composition and temperature; however, it is known that the lattice parameter in this family of alloys varies with composition [32]. It would be then expected a possible composition dependence of the interchange energies. Besides, since inhomogeneous microstructures are predicted at low temperatures, it is possible that size mismatch effects play a significant role. Another restriction of the model is that it was assumed that the Cu-Ni interactions are negligible; this is a reasonable simplifying assumption as a first approximation to the problem, but not necessarily correct. Further refinement of the model can be made by removing some of this restrictions; however, this will require the availability of more detailed experimental data. In particular, the experimental characterization of the atomic distribution in the $B2$ intermediate phase would be very interesting. Another possible method to gain understanding on the detailed nature of the ordering reactions would be based on the use of density functional theory (DFT) calculations. Combining DFT techniques with an appropriate inversion scheme [35,36], a set of effective pair (cluster) interactions can be obtained; the advantage of this method is that there is no need of fitting to experimental data.

Acknowledgements

This work was financially supported by ANPCyT, CONICET, SECAT-UNCPBA and CICPBA.

References

[1] Y. Nakata, T. Tadaki, K. Shimizu, Mater. Trans. JIM 31 (5) (1990) 652–658.
[2] J.I. Pérez-Landazábal, V. Recarte, R.B. Pérez-Sáez, M.L. Nó, J. Campo, J. San Juan, Appl. Phys. Lett. 81 (10) (2002) 1794–1796.
[3] V. Recarte, R.B. Pérez-Sáez, M.L. Nó, J. San Juan, J. Mater. Res. 14 (7) (1999) 2806–2813.
[4] V. Recarte, O.A. Lambri, R.B. Pérez-Sáez, M.L. Nó, J. San Juan, Appl. Phys. Lett. 70 (26) (1997) 3513–3515.
[5] R. Kainuma, X.J. Liu, I. Ohnuma, S.M. Hao, K. Ishida, Intermetallics 13 (2005) 655–661.
[6] J.L. Pelegrina, Phil. Mag. 94 (24) (2014) 2705–2723.
[7] G. Inden, Z. Metallkde. 66 (1975) 577–582;
G. Inden, Z. Metallkde. 66 (1975) 648–653.
[8] R. Rapacioli, M. Ahlers, Scr. Metall. 11 (1977) 1147.

[9] M. Ahlers, Philos. Mag. A 70 (1994) 247.
[10] R. Kikuchi, Phys. Rev. 81 (1951) 988.
[11] G. Inden, W. Pitsch, in: R.W. Cahn, P. Haasen, E.J. Kramer (Eds.), Materials Science and Technology: A Comprehensive Treatment, vol. 5, VCH, Weinheim, 1991.
[12] F. Lanzini, R. Romero, Comp. Mat. Sci. 96 (2015) 20–27.
[13] F. Ducastelle, Order and Phase Stability in Alloys, North-Holland, Amsterdam, 1991.
[14] T. Mohri, in: W. Pfeiler (Ed.), Alloy Physics: A Comprehensive Reference, Wiley-VCH Verlag, Weinheim, 2007.
[15] F. Lanzini, Doctoral Thesis, Universidad Nacional del Centro de la Provincia de Buenos Aires, Argentina, 2008.
[16] M. Jurado, Doctoral Thesis, Universitat de Barcelona, Spain, 1996.
[17] G. Inden, Acta Metall. 22 (1974) 945–951.
[18] K. Binder (Ed.), Monte Carlo Methods in Statistical Physics, Springer-Verlag, Berlin, 1987.
[19] O.G. Mouritsen, Computer Studies of Phase Transitions and Critical Phenomena, Springer-Verlag, Berlin, 1984.
[20] M. Blume, V.J. Emery, R.B. Griffiths, Phys. Rev. A 4 (1971) 1071.
[21] N. Metropolis, A. Rosenbluth, M.N. Rosenbluth, A.H. Teller, E. Teller, J. Chem. Phys. 21 (1953) 1087.
[22] S. Brodacka, M. Kozlowski, R. Kozubski, Ch. Goyhenex, G.E. Murch, Phys. Chem. Chem. Phys. 17 (2015) 28394–28406.
[23] J.L. Murray, Int. Met. Rev. 30 (1985) 211–233.
[24] F.R. de Boer, R. Boom, W.C.M. Mattens, A.R. Miedema, A.K. Niessen, Cohesion in Metals; Transition Metal Alloys, North-Holland, Amsterdam, 1988; A.R. Miedema, P.F. de Châtel, F.R. de Boer, Physica B 100 (1980) 1–28.
[25] F. Lanzini, P.H. Gargano, P.R. Alonso, G.H. Rubiolo, Model. Simul. Mater. Sci. Eng. 19 (2011) 015008.
[26] F. Lanzini, R. Romero, G.H. Rubiolo, Calphad 35 (2011) 396–402.
[27] F. Lanzini, R. Romero, M. Stipcich, M.L. Castro, Phys. Rev. B 77 (2008) 134207.
[28] E. Obradó, C. Frontera, Ll. Mañosa, A. Planes, Phys. Rev. B 58 (1998) 14245–14255.
[29] A. Alés, F. Lanzini, Model. Simul. Mater. Sci. Eng. 22 (2014) 085007.
[30] M. Jurado, T. Castán, Ll. Mañosa, A. Planes, J. Bassas, X. Alcobé, M. Morin, Phil. Mag. A 75 (1997) 1237–1250.
[31] F. Lanzini, R. Romero, M.L. Castro, Intermetallics 16 (2008) 1090–1094.
[32] R. Hu, H.-N. Su, P. Nash, Pure Appl. Chem. 79 (10) (2007) 1653–1673.
[33] Y. Nakata, Y. Iizuka, T. Ono, Mater. Trans. JIM 57 (3) (2016) 257–262.
[34] C.H. Chen, T.F. Liu, Mater. Chem. Phys. 78 (2002) 464–473.
[35] J.M. Sanchez, F. Ducastelle, D. Gratias, Physica A 128 (1984) 334.
[36] J.W.D. Connolly, A.R. Williams, Phys. Rev. B 27 (1983) 5169–5172.